Overdamped dynamics of paramagnetic ellipsoids in a precessing magnetic field

Pietro Tierno,* Josep Claret, and Francesc Sagués
Departament de Química Física, Universitat de Barcelona, Martí i Franquès 1, 08028 Barcelona, Spain

Andrejs Cēbers
Institute of Physics, University of Latvia, Salaspils-1, LV-2169, Latvia

(Received 9 September 2008; revised manuscript received 15 December 2008; published 5 February 2009)

We report on the dynamical behavior of paramagnetic ellipsoidal particles dispersed in water and floating above a flat plane when subjected to an external precessing magnetic field. When the magnetic field and the long axis of the particles are on the same plane, two clear regimes are distinguished in which the particles follow the magnetic modulation synchronously or asynchronously. Both regimes are also observed when the field precesses at an angle $\vartheta < 90°$ with respect to the normal to the confining plane, while the transition frequency increases with decreasing precession angle. We combine experimental observations with a theoretical model to characterize the particle dynamics. The possibility to control and/or reorient microscopic elongated particles by changing the frequency or strength of the applied field makes them suitable in microfluidic devices such as microgates for microchannels or active fluid mixers when placed close to channel junctions.

DOI: 10.1103/PhysRevE.79.021501 PACS number(s): 83.80.Gv, 47.57.J−, 05.60.Cd

I. INTRODUCTION

Elongated objects under external forcing, whether magnetic, electric, or vibrating, show fascinating dynamical behavior which is of interest for both fundamental and technological aspects. Externally vibrated springs represent a classical example leading to nonlinear dynamics and chaotic trajectories [1]. Magnetized rotating cylinders [2] or mechanically vibrated granular rods [3] provide the means to study general theories on dynamic self-assembly and collective organization in out-of-equilibrium systems. Regarding the practical aspect, one of the most common examples is the magnetic stir bar which is used in almost any chemical laboratory to efficiently mix different materials dispersed in a fluid. We also mention magnetic compasses, made of a magnetized tip that reorients with the earth's magnetic field and provide useful navigation data.

In overdamped systems, where the object dimensions become very small and viscous force dominates over inertia, novel phenomena can arise when dynamic fields are actuated over colloidal chains [4], microscopic rods [5], or flexible filaments [6]. In particular, there are different experimental procedures to deal with elongated particles in viscous fluids. Helgesen *et al.* [7] studied the dynamics of chains of magnetic "holes" (e.g., nonmagnetic particles dispersed in a ferrofluid) under rotating magnetic fields. Planar orientational motion of nanorods under electric [8] or optical [9] fields has also been described. Extensively studied are dynamic behaviors in rotating magnetic fields of chains of paramagnetic particles, unbound [10] or linked by functional molecules [11] or DNA bridges [12]. Similar studies extended to nanowire suspensions subjected to electric [13] or magnetic fields [14]. In all these cases the external driving is applied in the plane of the particles. Only very recently, Dhar *et al.* [15] showed that overdamped *ferromagnetic* nanorods, dispersed in water and floating above a flat plane, undergo a series of dynamical reorientations when subjected to a *precessing* magnetic field whose strength and frequency are independently varied.

In this work we study the dynamics of overdamped *paramagnetic* particles with *ellipsoidal* shape placed above a flat plane and subjected to various configurations of the external magnetic modulation. The elongated particles were prepared by stretching liquefied spherical colloids embedded in a polymeric deformable thin film. We distinguish between two situations depending on whether the applied magnetic field rotates in the plane or precesses around the normal to the particle plane. In both cases the particles show a transition from a synchronous to an asynchronous regime when the motion is nonlinear and the ellipsoids undergo a sequence of backward and forward motions. By tracking the particle's long and short axes projections on the plane, we characterize the orientational behavior and determine the critical frequency of the transition.

II. MATERIALS AND METHODS

Paramagnetic ellipsoidal particles were obtained by adapting the method of Ref. [16] to commercially available magnetite-doped un-cross-linked polystyrene microspheres (Micromod GmbH, Germany). These particles have mean radius $r=1.5$ μm (coefficient of variation $<5\%$), density of $\rho=1.1\times10^3$ kg/m^3 and a magnetic volume susceptibility $\chi \sim 0.4$ [17]. The particles were coated with surface carboxylic groups (COOH). A small suspension of these particles (50 mg/ml in water) was dispersed in a water solution containing 5% wt of polyvinyl alcohol (PVA) with glycerol (2%). The resulting solution was then cast into a thin film. After water evaporation, stripes of the film were cut and clamped into a metal frame [18]. The particles were liquefied by immersing the film with the frame into a beaker filled with toluene, and the film was slowly stretched along one direction. The frame was further removed from the solvent

*ptierno@ub.edu

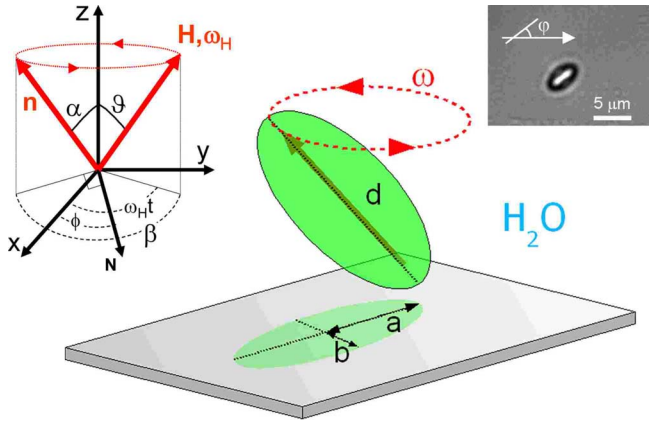

FIG. 1. (Color online) Schematic of a paramagnetic ellipsoidal particle (long axis d) floating above a glass plate and subjected to a magnetic field $\boldsymbol{H}$ which precesses with a frequency ω_H and an inclination ϑ around the z axis. a (b) denotes the projection of the particle long (short) semiaxis on the glass plane, while β is the phase lag angle between the projections on the plane of $\boldsymbol{n}$ and $\boldsymbol{H}$. The small inset on the right shows an optical microscope image of the particle, with the angle φ measured for counter-clockwise (ccw) rotation.

and left in air to allow the particles to solidify into ellipsoids. Finally, the film was repeatedly dissolved in a hot mixture of water and isopropanol and the particles collected with a permanent magnet. This procedure allows us to obtain paramagnetic particles with well-defined ellipsoidal shape, characterized by a long axis d (a is the projection on the plane of its semiaxis) and two equal short axes (semiaxis projection is b).

A water drop containing a diluted solution of the ellipsoids was deposited above a glass plate. After sedimentation ($\sim$5 min), the particles float a few nanometers above the plane due to the electrostatic repulsive interaction between their double layer (COO^-) and the negative silanol group ($-OH$) of the film. The external precessing magnetic field was provided by using three custom-made coils perpendicular to each other and having the main axes along the (x,y,z) directions. A rotating magnetic field in the particle plane was achieved by connecting two coils with the main axis along the (x,y) directions with a wave generator (TTi-TGA1244) feeding a power amplifier (IMG STA-800). A dc power supply (TTi-EL302Tv) was connected to the third coil to obtain a constant magnetic field along the z direction. The dynamics of the particles was recorded with a black and white Pixelink (PL-A741) charge-coupled device camera on a Nikon (E400) light microscope. By properly adjusting the camera settings we were able to record up to 250 frames/s under a 100× objective in a $\sim$100 μm^2 field of view containing one rotating particle.

To analyze the ellipsoid dynamics we measure two parameters: (1) the angle φ that the projection of the ellipsoid long axis d makes with a reference axis x (see the small inset in Fig. 1); (2) the average rotation frequency of the ellipsoid, $\bar{\omega}$. To measure both quantities we record AVI videos of the rotating particles by using a commercial frame-grabbing software (STREAMPIX, NORPIX). The videos were analyzed frame by frame with a custom-made program in MATLAB which uses the image processing toolbox. In particular, we load each frame as a jpeg image, filter it from noise and imperfections, adjust and enhance the image contrast, and finally obtain a black and white version of the corresponding image by using an appropriate threshold adjustment. We use two routines in the image processing toolbox: "Centroid," which finds the center of mass of the ellipsoidal region and "Orientation," which finds the angle between the x axis and the major axis of the ellipse. From the knowledge of both quantities, we extract the angle φ, which was continuously increased with time, and we determine $\bar{\omega}$ by measuring the rotation period of the ellipsoid during each field cycle and average its value over the acquisition time.

III. THEORETICAL MODEL

A prolate spheroidal particle [$p \equiv a/b > 1$ with a (b) the long (short) semiaxis] of volume $V_c = (4/3)\pi a b^2$ subjected to an external field $\boldsymbol{H}$ acquires a magnetic moment $\boldsymbol{m}$, which is related to $\boldsymbol{H}$ by $\boldsymbol{m} = \bar{\chi} V_c \boldsymbol{H}$, where $\bar{\chi}$ is a second-order tensor that denotes the magnetic susceptibility. In the case of an ellipsoidal particle with preferred magnetization along the director $\hat{\boldsymbol{n}}$, one can decompose $\bar{\chi}$ in terms of the susceptibility components parallel, $\chi_\parallel$, and perpendicular, $\chi_\perp$, to $\hat{\boldsymbol{n}}$. Thus $\bar{\chi} = \chi_\perp \bar{I} + \Delta\chi \hat{\boldsymbol{n}}\hat{\boldsymbol{n}}$, where $\Delta\chi = \chi_\parallel - \chi_\perp$ and $\bar{I}$ stands for the isotropic tensor. The magnetic field precesses at an angle ϑ around the z axis with frequency ω_H and strength $\hat{H}$, $\boldsymbol{H} \equiv \hat{H}(\sin\vartheta\cos(\omega_H t), \sin\vartheta\sin(\omega_H t), \cos\vartheta)$. For an arbitrary angle between $\boldsymbol{H}$ and $\hat{\boldsymbol{n}}$, one can write $\boldsymbol{m} = V_c[\chi_\perp \boldsymbol{H} + \Delta\chi(\boldsymbol{H}\cdot\hat{\boldsymbol{n}})\hat{\boldsymbol{n}}]$. The magnetic torque is obtained as $\boldsymbol{\tau}_m = \mu_w \boldsymbol{m} \times \boldsymbol{H} = \mu_w V_c \Delta\chi(\hat{\boldsymbol{n}} \times \boldsymbol{H})(\hat{\boldsymbol{n}} \cdot \boldsymbol{H})$. This torque is balanced by the viscous torque $\boldsymbol{\tau}_v = -\zeta_r \boldsymbol{\omega}$ arising from the rotation in the medium. Here μ_w is the magnetic susceptibility of water and ζ_r denotes the rotational friction coefficient of the rotating body. The equation of motion of the particle can be obtained from the balance of both torques:

$$\boldsymbol{\tau}_m + \boldsymbol{\tau}_v = \boldsymbol{0}, \tag{1}$$

where $\boldsymbol{n} \equiv (\sin\alpha\sin\phi, -\sin\alpha\cos\phi, \cos\alpha)$ and ϕ is the angle that the axis N normal to the projection of $\boldsymbol{n}$ on the plane makes with the x axis (see Fig. 1 for notation). If the external magnetic field rotates in the (x,y) plane, $\alpha = \vartheta = 90°$, we can project Eq. (1) along z, and obtain a single equation for the phase-lag angle $\beta = 90° + (\omega_H t - \phi)$:

$$\dot{\beta} = \omega_H - \omega_c \sin 2\beta, \tag{2}$$

where $\omega_c = \mu_0 V_c \Delta\chi H_\parallel^2 / 2\zeta_r$ and $H_\parallel = \hat{H}$. When the magnetic field precesses at a finite angle ($\vartheta < 90°$), we project Eq. (1) both in the plane and along z and obtain two equations for the angles α and β:

$$\dot{\alpha} = 2\omega_c \cos^2\alpha \cos^2\vartheta (1+\tilde{y}) \left(-\tan\alpha + \frac{\tilde{y}}{\tan\alpha} \right), \tag{3}$$

$$\dot{\beta} = \omega_H - 2\omega_c \cos\alpha \sin\alpha \cos\vartheta \sin\vartheta \sin\beta (1+\tilde{y}), \tag{4}$$

where $\tilde{y} = \tan\vartheta \tan\alpha \cos\beta$. Equation (4) can be further simplified by assuming $\alpha = \vartheta$ and obtaining

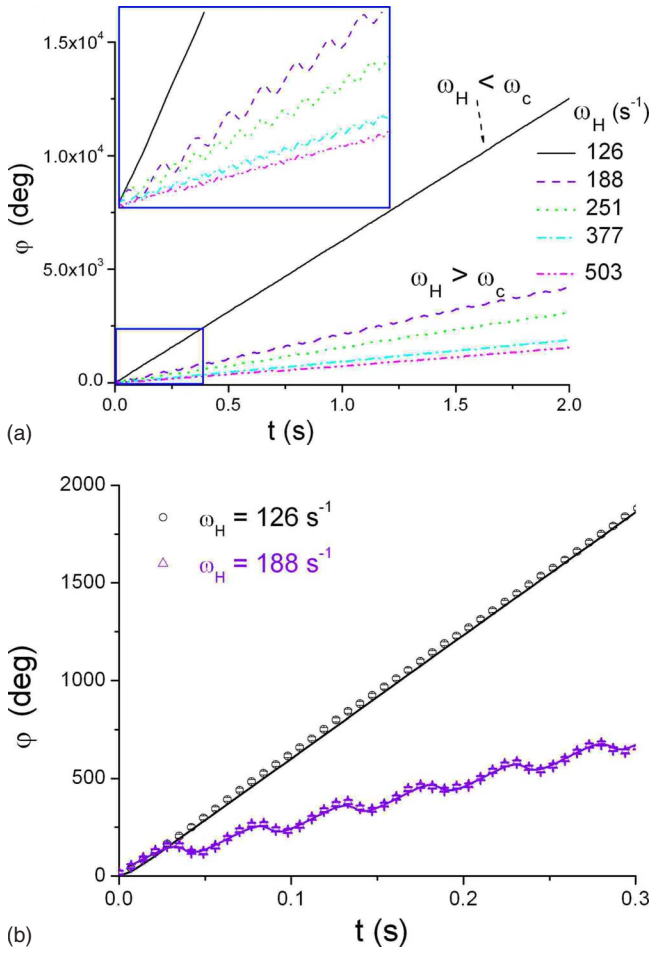

FIG. 2. (Color online) (a) Orientational angle φ versus time for different driving frequencies ω_H. ω_c indicates the critical frequency which distinguishes synchronous ($\omega_H<\omega_c$) from asynchronous ($\omega_H>\omega_c$) regimes. The small inset shows an enlargement of the diagram [0,0.4] s in t and [0°,2300°] in φ. (b) Continuous line is a numerical fit of the orientational data for $\omega_H=126$ s^{-1} ($\omega_H<\omega_c$) and 188 s^{-1} ($\omega_H>\omega_c$). The accuracy in the determined φ is 10°.

$$\dot{\beta} = \omega_H - \tilde{\omega}\frac{\sin\beta(1+\tan^2\vartheta\cos\beta)}{1+\tan^2\vartheta} \tag{5}$$

with $\tilde{\omega}=\mu_0 V_c \Delta\chi H_\parallel^2/\zeta_r$ and $H_\parallel=\hat{H}\sin\vartheta$.

IV. EXPERIMENTAL RESULTS

A. Ellipsoids under rotating magnetic field ($\vartheta=90°$)

We perform a first series of experiments by applying a magnetic field rotating in the particle plane ($\vartheta=90°$) and measure the orientations of the ellipsoidal particles as a function of the frequency and the strength. In this case we measure the angle φ that the projection on the plane of the particle long axis makes with the x axis, with the notation of Fig. 1, $\varphi=2\pi-(\pi/2-\phi)$. First we keep fixed the field amplitude to $\hat{H}=3200$ A/m and measure φ for different ω_H. Results for an ellipsoidal particle having an aspect ratio $p=a/b=1.5$ are shown in Fig. 2(a). When ω_H is lower than a critical value, $\omega_c=159$ s^{-1}, φ increases linearly with time and

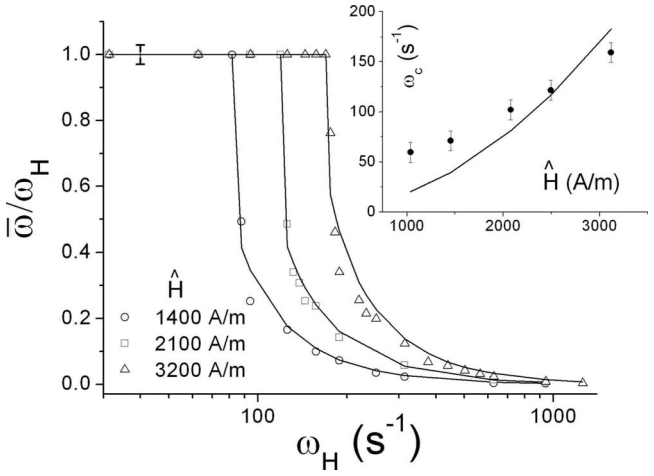

FIG. 3. Ellipsoid mean rotation frequency $\bar{\omega}$ normalized with respect ω_H versus the driving frequency ω_H for different strengths of the planar magnetic field $\hat{H}$. Continuous lines are linear fits for $\omega_H<\omega_c$ and fits which follow Eq. (6) for $\omega_H>\omega_c$. The single error bar is 0.03. The small inset shows the critical frequency ω_c versus $\hat{H}$ fitted with the function $\omega_c=f\hat{H}^2$ (see text). The accuracy in the determination of ω_c is 10 s^{-1}.

the ellipsoid rotates synchronously with the field, i.e., its angular velocity $\omega=\omega_H$. The motion is phase locked and the phase-lag angle β between $\boldsymbol{n}$ and $\boldsymbol{H}$ is constant. For driving frequencies higher than the critical frequency, φ shows time periodic oscillations [see Fig. 2(a)] which correspond to a characteristic "back-and-forth" motion of the ellipsoid during each cycle. In this case the driving field rotates faster than the particle and the angle β is no longer constant. In particular, when the rotating field surpasses the ellipsoid, the director $\boldsymbol{n}$ tries to follow $\boldsymbol{H}$, which results in a forward rotation, $\dot{\beta}>0$. When the angle $\beta>90°$, $\boldsymbol{n}$ is in front of the field and the ellipsoid moves backward in order to align with the field $\boldsymbol{H}$. This influences the particle motion and reduces the average rotation frequency of the ellipsoid. It should be noted also that these backward rotations could eventually arrest the particle motion at very high frequency, but never lead to a reverse average rotation with respect to the magnetic field handedness [19]. In terms of the angle φ, Eq. (2) becomes $\dot{\varphi}=\omega_c\sin[2(\omega_H t-\varphi)]$. We fit the orientational data for $\omega_H<\omega_c$ and $\omega_H>\omega_c$ by using the solutions of this differential equation. Two of these fits are presented in Fig. 2(b) for $\omega_H=126$ and for 188 s^{-1}. We obtain in both cases $\omega_c=132$ s^{-1}, which differs by ~30 s^{-1} from the experimentally determined value. Due to this uncertainty related to the determination of the critical frequency, we adopt an alternative way to theoretically match ω_c.

The critical frequency can be determined directly by recording the particle rotation and measuring the average angular frequency $\bar{\omega}$ of the ellipsoid at different ω_H. Such measures for different strengths of the applied field $\hat{H}$ are reported in Fig. 3. Below ω_c, $\bar{\omega}$ is linear with ω_H, while for $\omega_H>\omega_c$ the particle rotational motion decreases with increasing ω_H. The average rotation frequency can be obtained as $\bar{\omega}=\lim_{T\to\infty}(1/T)\int_0^T\dot{\varphi}\,dt$ where T is the period, and it results in [20]

$$\frac{\bar{\omega}}{\omega_H} = 1 - \sqrt{1 - \left(\frac{\omega_c}{\omega_H}\right)^2}. \quad (6)$$

We use this equation to fit the experimental data in the $\omega_H > \omega_c$ region and determine the value of the critical frequencies with an error less than 10 s^{-1}. In the small inset of Fig. 3 such values are plotted versus $\hat{H}$ and fitted with the ansatz $\omega_c = f\hat{H}^2$ which gives $f = 0.2 \times 10^{-4}$ m^2 A^{-2} s^{-1}. We can use this value to estimate the rotational friction coefficient of the ellipsoidal particle ζ_r if we know the magnetic susceptibility anisotropy $\Delta\chi$. To estimate $\Delta\chi$, we write the magnetic particle susceptibilities $\chi_\parallel$ and $\chi_\perp$ in terms of their shape-dependent demagnetization factors $N_\parallel$ and $N_\perp$, from which we obtain $\Delta\chi = \chi[1/(1+N_\parallel\chi) - 1/(1+N_\perp\chi)]$. Both demagnetization factors $N_\parallel$ and $N_\perp$ depend on the ellipsoid geometry and thus on p. For a prolate spheroid with $p > 1$, exact expressions have been calculated a long time ago in [21]. If we use $\mu_w \sim \mu_0 = 4\pi \times 10^{-7}$, H/m $V_c = 1.4 \times 10^{-17}$ m^3, and $\Delta\chi = 0.019$ we estimate a friction coefficient of $\zeta_r = 0.8 \times 10^{-20}$ N s m for $p = 1.5$. As shown in Fig. 3, the effect of the magnetic field strength on $\bar{\omega}$ is to shift the position of the critical frequency. The influence of Brownian fluctuations becomes non-negligible at lower strength ($\hat{H} < 10^3$ A/m) and perturbs the particle motion. To avoid interference of such fluctuations, we perform the next series of experiments at fixed magnetic field $\hat{H} = 3200$ A/m.

B. Ellipsoids with different aspect ratios $p > 1$

In the previous section we analyzed the dynamic behavior of one ellipsoidal particle under a rotating magnetic field by varying the field frequency and strength. Since the method described in Sec. II allows us to prepare ellipsoidal particles with different aspect ratios p, we here investigate how this parameter affects the particle dynamics.

In Fig. 4(a) we show the average rotation frequency for ellipsoidal particles with different aspect ratios, from $p = 1.2$ to 4.2. The corresponding microscope images, ordered from the higher to the lower p, are shown as a small inset in the image. We determine ω_c for different p by fitting the experimental data with Eq. (6) in the region $\omega_H > \omega_c$. It follows that an increase in the aspect ratio corresponds to a decrease in the critical frequency and thus to a lower maximum angular speed achievable by the particles. This is due to the increase in the viscous torque required to rotate longer ellipsoidal particles with a consequently smaller axis of rotation. The critical frequency depends inversely on the rotational friction coefficient, $\omega_c \sim 1/\zeta_r$ which in turn depends on the geometry of the ellipsoidal particle. For a prolate ellipsoid rotating around its short axis, the friction coefficient has been precisely calculated in Refs. [23–25] and its value can be written as $\zeta_r = 8\pi\eta V_c f_r$, where r is the radius of the original undeformed sphere [26], and f_r is a geometrical factor which depends on the parameters a and b [22]. Instead, for a rotating sphere the friction coefficient is simply $\zeta_r = 8\pi\eta r^3$. We first estimate ζ_r directly, by determining the critical frequency from the data in Fig. 4(a). These values of ω_c versus p are shown in the small inset of Fig. 4(b). The extracted

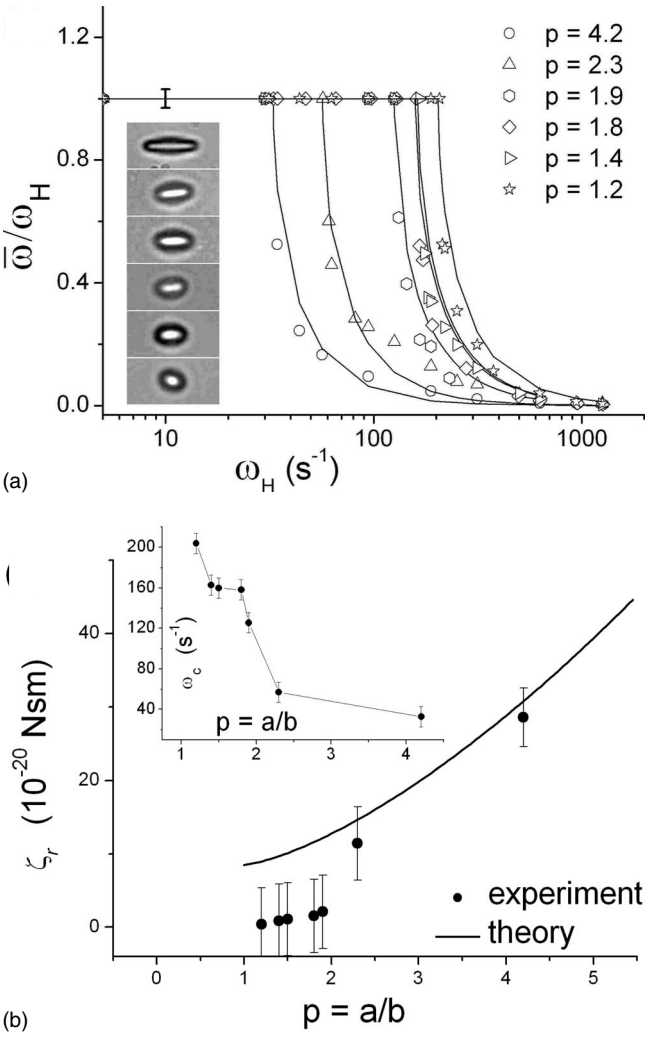

FIG. 4. $\bar{\omega}/\omega_H$ versus the driving frequency ω_H for ellipsoidal particles with different aspect ratios $p = a/b$, from $p = 1.2$ to 4.2 where a (b) denotes the long (short) semiaxis. On the left we show microscope images of the ellipsoidal particles ordered from $p = 4.2$ to 1.2. (b) Rotational friction coefficient ζ_r of the ellipsoidal particles versus p. The continuous line is the theoretical calculation from [22]. The small inset shows the critical frequencies ω_c versus p extracted from the data in (a).

values of ζ_r (closed circles) versus p are plotted in Fig. 4(b). We note that increasing the ellipsoid aspect ratio p increases the magnetic susceptibility anisotropy from $\Delta\chi = 0.01$ for $p = 1.2$ to $\Delta\chi = 0.05$ for $p = 4.2$. Together with the experimental data, we show as a continuous line the theoretical calculation of ζ_r. The agreement between the data and the continuous line is within the experimental errors. We have also to notice that in our estimation we neglect the hydrodynamic interaction of the rotating particle with the plane. It has been shown that, for cylindrical particles with large aspect ratio (p from 4 to 30), such interaction could be as higher as ~25% of the total viscous torque [8]. However, since the aspect ratio of our particle is smaller, $p < 4$, and the hydrodynamic shape is different from the cylindrical one, this quantity is even smaller and can be included in our error analysis.

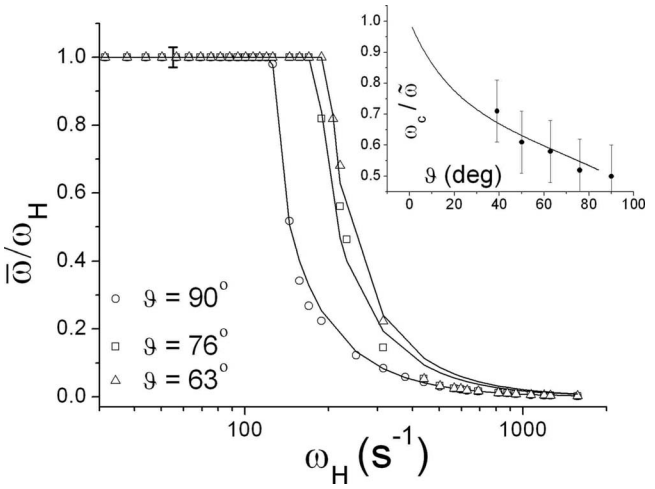

FIG. 5. Averaged ellipsoid rotation frequency $\bar{\omega}/\omega_H$ versus ω_H for different precession angles ϑ ($H_\parallel$ is kept constant). The small inset shows the ratio $\omega_c/\bar{\omega}$ versus ϑ while the continuous curve was obtained from Eq. (7) as indicated in the text.

C. Ellipsoids under precessing magnetic field ($\vartheta < 90°$)

When the external field precesses at an angle ϑ with respect to the z axis, two dynamical regimes appear, corresponding again to synchronous and asynchronous motions with respect to the external field. The orientational behavior of the ellipsoid long axis is similar to the case $\vartheta = 90°$ reported in Fig. 2, and thus is not shown here. In Fig. 5 we show the values of $\bar{\omega}/\omega_H$ versus ω_H for different precession angles ϑ. When ϑ decreases, the critical frequency increases and doubles for $\vartheta \sim 0°$ with respect to $\vartheta = 90°$. The equations describing the ellipsoidal dynamics correspond to the orientational [α, Eq. (3)] and azimuthal motion [β, Eq. (4)]. If we assume we are in the synchronous regime, where $\dot{\beta} = 0$, Eq. (5) can be further reduced to

$$F(t, \omega_H/\tilde{\omega}, \tan^2\alpha) = \frac{\omega_H}{2\tilde{\omega}}(1+\tan^2\alpha)(1+t^2)^2 - 2t[1+t^2+\tan^2\alpha(1-t^2)] = 0, \quad (7)$$

where $t = \tan(\beta/2)$. The steady state exists if Eq. (7) has real solutions for t.

For the critical values of parameters, i.e., in the limit of the synchronous regime, we have $F(t, \omega_c/\tilde{\omega}, \tan^2\alpha) = 0$ and $dF(t, \omega_c/\tilde{\omega}, \tan^2\alpha)/dt = 0$. In the small inset of Fig. 5, the numerical solutions of these equations are plotted together with the experimental data. During these experiments the planar component of the magnetic field, $H_\parallel$, was kept always constant, and to decrease ϑ, the strength of the static magnetic field applied normal to the film was increased. This comparison shows the good agreement with the experimental data and validates our model even if more complicated effects like interactions of the particle with the plate are not taken into account.

V. CONCLUSIONS

We prepared anisotropic paramagnetic colloidal particles and investigated their dynamical behavior when subjected to an externally modulated magnetic field. The particle orientations in real space were explored for different strength, frequency, and precession angle of the magnetic field. We complement the experimental analysis with a model which allows us to describe the particle behavior. Although our model does not consider the effect of the surface above which the particles float, it captures the essential ingredients needed to interpret their motion in terms of the orientational angle and critical frequency.

Controllable motion of microscopic elongated particles, like our paramagnetic ellipsoids, is very appealing for application in microscale devices. For example, Terray *et al.* [27] showed that optical trapped chains of silica particles dispersed into customized microscopic channels can be used as active fluid elements (pumps or valves) to displace fluids. Bleil *et al.* [28] placed microscopic colloidal pumps into a microfluidic network by rotating a few paramagnetic spherical particles with external magnetic fields. Magnetic fields allow further miniaturization of integrated devices since there are no limitations imposed by light diffraction. Also, chains of paramagnetic particles have been employed as mechanical stirrers for confined fluid applications [11,29]. In the last case, filament bending [30,31] could limit the mixing efficiency at high frequencies and even produce rupture of the filament. Rigid elongated particles, like the ones presented here, could avoid this problem. Investigation in this direction will be the subject of future work.

ACKNOWLEDGMENTS

P.T. was supported by the program Beatriu de Pinós Grant No. BP-B100167. P.T., J.C., and F.S. acknowledge financial support by MEC (Project No. FIS2006-03525) and DURSI (Project No. 2005SGR00653). A.C. is thankful for financial support by the University of Latvia (Grant No. Y2-ZP10-100).

[1] F. C. Moon, *Chaotic Vibrations: An Introduction for Applied Scientists and Engineers* (Wiley-VCH, Berlin, 2004).
[2] B. A. Grzybowski and G. M. Whitesides, Science **296**, 718 (2002).
[3] V. Narayan, S. Ramaswamy, and N. Menon, Science **317**, 105 (2007).
[4] S. Melle, O. Calderòn, M. A. Rubio, and G. G. Fuller, Int. J. Mod. Phys. B **16**, 2293 (2002).
[5] B. Qian, T. R. Powers, and K. S. Breuer, Phys. Rev. Lett. **100**, 078101 (2008).
[6] M. Belovs and A. Cēbers, Phys. Rev. E **73**, 021507 (2006).
[7] G. Helgesen, P. Pieranski, and A. T. Skjeltorp, Phys. Rev. Lett. **64**, 1425 (1990).
[8] B. Edwards, T. S. Mayer, and R. B. Bhiladvala, Nano Lett. **6**,

626 (2006).
[9] W. A. Shelton, K. D. Bonin, and T. G. Walker, Phys. Rev. E **71**, 036204 (2005).
[10] S. Melle, G. G. Fuller, and M. A. Rubio, Phys. Rev. E **61**, 4111 (2000).
[11] S. L. Biswal and A. P. Gast, Phys. Rev. E **69**, 041406 (2004).
[12] R. Dreyfus, J. Baudry, M. L. Roper, M. Fermigier, H. A. Stone, and J. Bibette, Nature (London) **437**, 862 (2005).
[13] D. L. Fan, F. Q. Zhu, R. C. Cammarata, and C. L. Chien, Phys. Rev. Lett. **94**, 247208 (2005).
[14] K. Keshoju, H. Xing, and L. Sun, Appl. Phys. Lett. **91**, 123114 (2007).
[15] P. Dhar, C. D. Swayne, T. M. Fischer, T. Kline, and A. Sen, Nano Lett. **7**, 1010 (2007).
[16] J. A. Champion, Y. K. Katare, and S. Mitragotri, Proc. Natl. Acad. Sci. U.S.A. **104**, 11901 (2007).
[17] R. Wirix-Speetjens, W. Fyen, J. D. Boeck, and G. Borghs, J. Appl. Phys. **99**, 103903 (2006).
[18] C. C. Hol, A. Keller, J. A. Odell, and R. H. Ottewill, Colloid Polym. Sci. **271**, 469 (1993).
[19] K. Ērglis, Q. Wen, V. Ose, A. Zeltins, A. Sharipo, P. Janmey, and A. Cēbers, Biophys. J. **93**, 1402 (2007).
[20] S. Lācis, J. C. Bacri, A. Cēbers, and R. Perzynski, Phys. Rev. E **55**, 2640 (1997).
[21] J. A. Osborn, Phys. Rev. **67**, 351 (1945).
[22] $f_r=(a^2+b^2)/(a^2n_1+b^2n_2)$ with $n_1=[2\pi(1-e^2)/e^3]\{\log[(1+e)/(1-e)]-2e\}$, $n_2=(1/2)(4\pi-n_1)$, $e=\sqrt{1-(b/a)^2}$ is the ellipse eccentricity, and a (b) denotes the long (short) semiaxis.
[23] F. Perrin, J. Phys. Radium **5**, 497 (1934).
[24] F. Perrin, J. Phys. Radium **7**, 1 (1936).
[25] S. Koenig, Biopolymers **14**, 2421 (1975).
[26] During the fabrication of the ellipsoidal particle the volume can be considered constant and the radius of the original undeformed particle can be related to the aspect ratio p as $r=bp^{1/3}$.
[27] A. Terray, J. Oakey, and D. W. M. Marr, Science **296**, 1841 (2002).
[28] S. Bleil, D. W. M. Marr, and C. Bechinger, Appl. Phys. Lett. **88**, 263515 (2006).
[29] R. Calhoun, A. Yadav, P. Phelan, A. Vuppu, A. Garcia, M. Hayes, L. Gabrielson, and M. J. Folkes, Lab Chip **6**, 247 (2006).
[30] C. Goubault, P. Jop, M. Fermigier, J. Baudry, E. Bertrand, and J. Bibette, Phys. Rev. Lett. **91**, 260802 (2003).
[31] A. Cēbers and I. Javaitis, Phys. Rev. E **69**, 021404 (2004).